Optics Communications 488 (2021) 126853

Contents lists available at ScienceDirect

Optics Communications

journal homepage: www.elsevier.com/locate/optcom

Octave-spanning coherent supercontinuum generation in a step-index tellurite fiber and towards few-cycle pulse compression at 2 μm

B. Kibler [a,*], A. Lemière [a], J.-T. Gomes [b,1], D. Gaponov [b], L. Lavoute [b], F. Désévédavy [a], F. Smektala [a]

[a] Laboratoire Interdisciplinaire Carnot de Bourgogne, UMR 6303 CNRS-Université de Bourgogne Franche-Comté, 21078 Dijon, France
[b] Novae, 15 rue Sismondi, 87000 Limoges, France

ARTICLE INFO

Keywords:
Nonlinear fiber optics
Supercontinuum generation
Pulse compression
Infrared fibers

ABSTRACT

We experimentally demonstrate 140-THz bandwidth (at −20 dB) supercontinuum generation in a 10 cm-long all-normal dispersion step-index tellurite fiber pumped by a turn-key femtosecond fiber laser emitting at 2.11 μm at a repetition rate of 19 MHz. The soliton self-frequency shifted thulium-doped fiber mode-locked laser emits initial transform-limited pulses, with 85-fs pulse duration, that are subsequently quasi-linearly chirped (over more than 50 THz) during the above nJ-level nonlinear propagation. Moreover, we numerically demonstrate the possible pulse compression down to 12 fs by means of additional linear propagation in a standard step-index fluoride fiber with anomalous dispersion.

1. Introduction

The development of compact fiber-based supercontinuum (SC) light sources has undergone a dramatic increase, in particular spanning the mid-infrared (mid-IR) molecular fingerprint region (2–12 μm) for spectroscopy and microscopy [1–5]. Such fiber SC sources based on fluoride, tellurite, or chalcogenide optical fibers result from extreme spectral broadening of high intensity pump laser pulses through a combination of instantaneous (Kerr) and delayed (Raman) nonlinear processes [6–10]. Such demonstrations were initially performed using large high-power femtosecond lasers with low repetition rate and average power. However, in the past few years, there has been a surge of interest in novel compact mid-IR optical materials and lasers [11,12], so that very compact commercial mid-IR femtosecond fiber lasers are now available and can be used as pump lasers between 2 and 4 μm for developing a robust all-fiber SC module [13–16]. In general, the exploitation of compact and robust fiber SC schemes with improved coherence and flatness could be advantageous for applications like absorption spectroscopy or pulse recompression [17,18], but still requires considerable efforts beyond 2 μm to reach the remarkable efficiency already demonstrated in the near-IR. To this regard, several experimental attempts have been already reported in the important spectral transition between near-IR and mid-IR (1.5–3.5 μm) [13,19–24] by using normal dispersion fibers made of chalcogenide or tellurite glasses. Note that only Refs. [13,19] are based on pumping with a compact fiber laser, then coupled into chalcogenide fibers. We previously demonstrated that step-index tellurite fibers are suitable candidates in this spectral region, in particular through their dispersion characteristics and their ability to control frequency conversion and supercontinuum generation with 2 μm pump lasers [25,26]. However, their combination with compact femtosecond lasers beyond 2 μm for coherent SC generation has not been reported so far.

In this manuscript, we demonstrate the generation of quasi-linearly chirped supercontinuum pulses using a short segment of all-normal dispersion (ANDi) tellurite fiber. Pumped with a 2.11 μm fiber laser, we achieve through self-phase modulation and optical wave-breaking a -20 dB bandwidth from 1.3 to 3.4 μm and a - 3 dB bandwidth from 1.5 to 3 μm (100 THz) at 20 kW coupled peak power (33 mW average power). Such spectral bandwidths and average power clearly exceed the capabilities reported in Ref. [19] with the same fiber laser and a chalcogenide fiber. Our experimental results are confirmed by numerical simulations based on the generalized nonlinear Schrödinger equation (GNLSE) for distinct pumping powers. Next, we numerically investigate the subsequent stage of temporal compression of the above positively chirped pulses in a standard fluoride fiber through dispersion-induced recombination of frequency components. Optimization procedure of both fiber lengths (nonlinear and linear stages of propagation) is analyzed to achieve the maximum compression factor according to the minimum of the time-bandwidth product and pulse deformation. Based on the coupled peak power in the nonlinear stage, we find that optimized fiber lengths allow to reach the few-optical-cycle regime of the underlying electric field.

* Corresponding author.
E-mail address: bertrand.kibler@u-bourgogne.fr (B. Kibler).
[1] Now at Leukos, 2 rue Edouard Michaud Beaublanc, Bât. 3-4-5, 87000 Limoges, France.

https://doi.org/10.1016/j.optcom.2021.126853
Received 20 December 2020; Received in revised form 2 February 2021; Accepted 5 February 2021
Available online 9 February 2021

2. Experiments

2.1. Fiber properties and experimental setup

Our step-index tellurite fibers for mid-IR SC generation are developed through the build-in-casting and the rod-in tube techniques which are well described in our previous works [26,27]. In particular, core and cladding glasses were chosen based on their optical, thermal and mechanical compatibility for the build-in-casting process, and suitable refractive index difference (about 0.1 at 2 μm) for light guidance through a simple step-index design. The corresponding compositions are respectively $80TeO_2$-5ZnO-$10Na_2O$-$5ZnF_2$ (TZNF, molar fraction) and $60TeO_2$-5ZnO-$20Na_2O$-$15GeO_2$ (TZNG). The synthesis and quenching of the glass preform are performed in a glove box under dry atmosphere to avoid any water contaminations from the environment. To further reduce the presence of hydroxyl compounds and limit the mid-IR absorption of the fiber, zinc fluoride is added to the core composition [28]. TZNF and TZNG glasses are synthesized from high purity precursors. Both melted glasses are quenched in a pre-heated cylindrical brass mold and then annealed. We obtain a 45 mm long and 16 mm large cylindrical preform inside which it is easy to differentiate the two different compositions as shown in the inset of Fig. 1a. The resulting step-index glass preform is drawn into capillaries with an outer diameter of 800 μm for the next rod-in-tube stage. A second cladding glass preform used as a tube is made by following the protocol above described and drilled mechanically. The step-index rod is then inserted into the hole of the second cladding tube and another drawing stage is performed to obtain small-core step-index fibers varying between 3 and 6 μm. Typically, our fibers exhibit background losses below 1 dB/m between 1 and 2.8 μm, and the water-related absorption band around 3 μm remains below 2 dB/m (see Fig. 1a). Fiber losses then increase and reach the multiphonon absorption edge beyond 4 μm. Such losses were measured over the entire wavelength range by means of the cutback method on 8-m-long samples of large-core step-index fiber (50 μm core diameter) and using a blackbody source. Similar loss values were only confirmed at particular wavelengths (1.55 and 2 μm) in small-core fibers since requiring narrow linewidth lasers with a higher power due to low-coupling issues. However, we verify that losses still remain moderate up to 4 μm when considering cm-long segments of small-core fibers as demonstrated in Ref. [7].

As studied in our previous works [25,27], based on this simple step-index profile, our fibers do not exhibit a strictly single-mode behavior in the mid-IR spectral range, but high numerical apertures and a rather strong confinement of the fundamental guided mode. Calculated dispersion curves and effective mode area variations as a function of wavelength of the fundamental guided mode are shown in Fig. 1b-1c (obtained by solving the eigenvalue equation for cylindrical step-index waveguides). Our fiber design provides distinct dispersive regimes by simply varying the core diameter from 3 to 3.5 μm, namely all-normal dispersion profile and multi-zero dispersion wavelength profile. In particular, we find that anomalous dispersion only exists for core diameters larger than 3.25 μm. The flexibility of dispersive properties beyond 2 μm combined with strong optical confinement allowed us to investigate an overview of some relevant nonlinear dynamics of SC generation, in both picosecond and femtosecond pumping regimes at moderate peak powers [7,25,26]. Here we focus our study on the femtosecond pumping regime and the all-normal dispersion regime for generating quasi-linearly chirped supercontinuum pulses with significant powers and their application for pulse recompression.

We made use of a simple configuration of SC generation experimental setup described as follows: (i) The pump source is a commercial, turn-key soliton self-frequency shifted thulium-doped fiber mode-locked laser (NOVAE Brevity λ+). The delivered transform-limited pulses, centered at 2.11 μm with repetition rate of 19 MHz and average power of about 200 mW, exhibit a duration at full width half maximum (FWHM) of 85 fs (i.e., 4 THz spectral bandwidth). Here our study was performed with the free-space output option (i.e., collimated Gaussian beam) of the fiber laser to avoid any damage of output fiber facet during optimization procedures. However, note that for more robust SC schemes, suitable splicing methods could be used to directly connect the tellurite fiber with the fiber output of the femtosecond laser. (ii) Before coupling into the tellurite fiber, both linear polarization and input power of pump pulses are controlled via the combination of a half-wave plate and a variable optical attenuator (90% total transmission). (iii) Our small-core tellurite fibers were cleaved by means of a scalpel blade and quality of the interfaces was carefully checked under microscope (see Ref. [26]) before mounting a few-cm long fiber sample onto a 3-axis holder. Pump pulses are then coupled into the fundamental mode of the tellurite fiber under study by using a standard aspheric lens (4 mm focal length and 90% transmission). Our coupling efficiency is about 20% for our small-core fibers, so that SC generation can be investigated with a maximum input peak power of roughly 20 kW (33 mW average power). (iv) At the output of such tellurite fibers (featured by high numerical apertures [27]), the SC light is directly collected by a 0.5-m long multimode fluoride (InF_3) fiber with the butt-coupling technique. This multimode fiber (100 μm core) facilitates the collection stage of the SC light and exhibits an excellent transmission over the 0.35–5.5 μm spectral range. Finally, the SC light is collimated by means of an off-axis parabolic gold mirror and directly sent to the FTIR spectrometer spanning the 1–5 μm range.

2.2. Results of supercontinuum generation

In this subsection, we present the experimental results of SC generation in two step-index tellurite fibers, namely with all-normal dispersion (3.15 μm core diameter) and with two zero-dispersion wavelengths (3.45 μm core diameter). We provide this comparison to highlight the impact of dispersive properties on the resulting output SC spectrum and its -20 dB bandwidth. Fig. 2 shows the recorded output spectra for both types of fiber as a function of input peak power. We here fixed the fiber lengths to 10 cm. Based on our previous study of SC generation with similar fs pulse pumps [26], it was demonstrated that the maximum spectral broadening is usually reached for such fiber segments. Numerical simulations will confirm this hypothesis in the next section.

Pumping in the normal dispersion regime (see Fig. 2a) implies that SC generation is mainly driven by self-phase modulation (SPM) and optical wave-breaking [29], thus the spectrum remains nearly symmetric around the pump wavelength and narrower than in other dispersion regimes. The typical features of SC generation in ANDi fibers are (i) the spectral flatness, (ii) the single-pulse preservation and its quasi-linear chirping, and (iii) the stability to input noise, which guarantees a full SC coherence [30–32]. Optical wave-breaking is an important phenomenon affecting short pulse dynamics in the normal dispersion, which creates new frequencies through four-wave mixing and enhances the flatness of the central part of the spectrum. The spectrum is also associated with a nearly linear distribution of the instantaneous frequency across the pulse. In general, the frequency chirp is maximal before wave-breaking has occurred (dominant SPM) and, after that, accelerated pulse broadening takes place. To achieve the largest spectrum with high spectral flatness, it is convenient to propagate the input pulse until wave-breaking occurs. Then, one can use the empirical L_D/N scaling of wave-breaking distance L_{WB} to ensure the saturation of the pulse spectral broadening. Moreover, a rough estimate of the maximum spectral broadening for secant-hyperbolic pulses can be found as 1.7 N [29]. Note that such simple rules were derived assuming a dispersion flattened fiber (i.e., neglecting higher-order dispersions) and without higher-order nonlinear effects such as the self-steepening effect. Here, N is defined as $N = \sqrt{L_D/L_{NL}}$ with the dispersion length $L_D = T_0^2/|\beta_2|$ and the nonlinear length $L_{NL} = 1/\gamma P_0$, where P_0 is the input peak power, T_0 is the half-width (at 1/e-intensity point) of the input pulse, β_2 and γ are respectively the fiber group-velocity dispersion

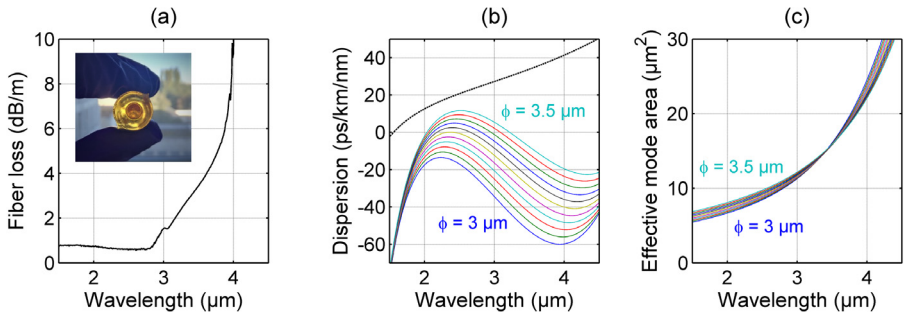

Fig. 1. (a) Fiber loss measured by means of the cutback method in a large-core step-index fiber (inset: Cross-section of the step-index preform). (b–c) Wavelength-dependent curves of dispersion D and effective mode area of the fundamental guided mode of step-index tellurite fibers with distinct core diameters from 3 to 3.5 μm by step of 50 nm. The black curve in panel (b) shows the dispersion of the 14 μm-core ZBLAN fiber used for pulse compression.

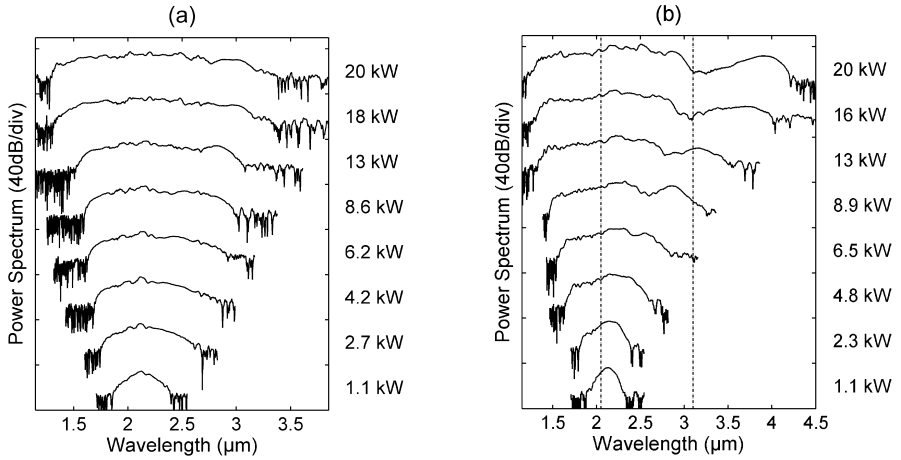

Fig. 2. Evolution of SC spectrum recorded experimentally as a function of input peak power for 10-cm-long tellurite fiber segments with (a) all-normal dispersion and (b) two zero-dispersion wavelengths. The dotted lines indicate the positions of calculated zero dispersion wavelengths.

and the fiber nonlinear coefficient at the pump wavelength λ_0. In our experimental configuration, $\beta_2 = -D\lambda^2/2\pi c = 18$ ps ^{2} km^{-1} (c is the speed of light) and $\gamma = 153$ W^{-1} km^{-1}. We find that all our SC spectra recorded after 10 cm of propagation (whatever the input peak power) are obtained well-beyond the optical wave-breaking has occurred (see Fig. 2a). This implies that the maximal spectral broadening is also reached. For example, in the case of $P_0 = 8.6$ kW, $N \sim 13$ and $L_D \approx 13$ cm, so that $L_{WB} \sim 1$ cm and the spectral broadening factor is about 22 times the initial 4 THz spectral width (i.e., 88 THz). Experimentally, the corresponding SC spectrum spans from 1.65 to 2.9 μm, which corresponds to 78 THz. For the highest input peak power (33 mW average power), we achieve a −20 dB bandwidth from 1.3 to 3.4 μm (i.e., 140 THz). Such spectral bandwidths and associated average powers clearly exceed the capabilities reported experimentally in Ref. [19] with the same fiber laser and a chalcogenide fiber, as well as numerical predictions of ANDi SC generation in step-index fluoride fibers around 2 μm [33].

For comparison, in Fig. 2b, we show the pumping in the anomalous dispersion regime between two close zero-dispersion wavelengths (at 2.05 and 3.1 μm), which leads to broader SC spectra. In that case, the spectral broadening results from well-known soliton dynamics and Raman soliton-self-frequency shift [26,30]. We can note that both edges of the SC spectrum for high pump powers are formed by dispersive waves in both regions of normal dispersion, namely in the near-IR below 2 μm and in the mid-IR beyond 3.1 μm. This pumping regime with low anomalous dispersion and two close zero-dispersion wavelengths implies typical features such as, the broadest SC spectrum, its multi-pulse nature, its lower spectral flatness, higher sensitivity to input noise for N values beyond 10 (most of the spectra reported in Fig. 2b), and thus the degradation of SC coherence [26].

In the following we focus on the detailed analysis of our ANDi SC spectra by means of numerical simulations in terms of spectral bandwidth and chirp, and their possible use for subsequent pulse compression towards the few-optical cycle regime.

3. Numerical simulations

3.1. Linearly chirped supercontinuum pulses

We first performed numerical simulations of the nonlinear pulse propagation in our tellurite fiber with all-normal dispersion to confirm the experimental SC bandwidths measured above, accordingly to the pumping parameters. Our modeling is based on the generalized nonlinear Schrödinger equation that includes the full dispersion curve of the fundamental mode, both instantaneous Kerr and delayed Raman nonlinear responses, and the dispersion of nonlinearity [30]. This equation governs the evolution of the complex envelope of the electrical field. For the Raman response function, we used an intermediate-broadening model using convolutions of Lorentzians and Gaussians adapted from spontaneous Raman scattering spectra and estimated Raman gain coefficient given in Ref. [34]. The contribution of the delayed Raman response was found to be $f_R = 0.25$. Our simulations also include the fiber losses measured in Fig. 1. The dependence of SC stability on the input pulse characteristics and the fiber parameters has been extensively studied during the last decade [30,32]. The use of ANDi fibers allows highly coherent SC to be designed for pump pulses equivalent to $N \sim 600$ and pulse duration up to 1.5 ps.

The sensitivity of SC fluctuations to input noise will be studied in the following, as described in Ref. [30], namely by performing 100 simulations with different random input noise imposed on the input

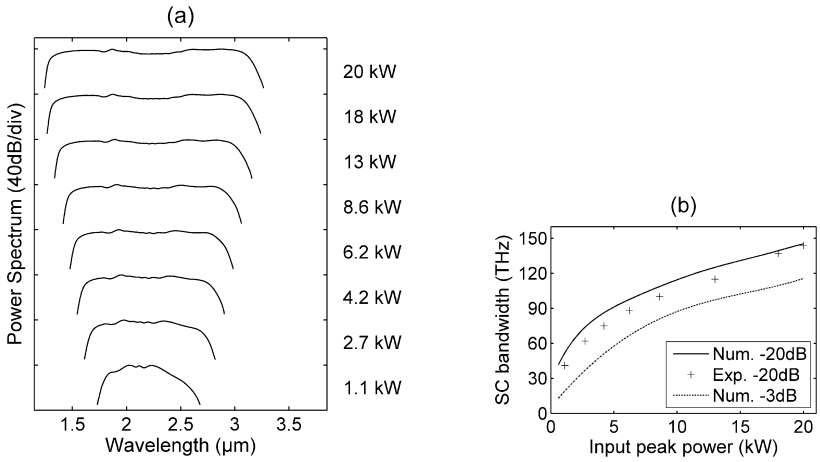

Fig. 3. (a) Evolution of SC spectrum obtained from simulations as a function of input peak power for the 10-cm-long ANDi tellurite fiber (Spectral dynamics is shown over 35 dB only for an easier comparison with experiments). (b) Comparison of −20 dB SC bandwidth obtained experimentally (crosses) and numerically (solid line). Dotted line indicates the numerical −3 dB SC bandwidth.

pulse for each fiber. The ensemble of output SC fields allows the calculation of the complex degree of first-order coherence over the SC spectrum $g_{12}^{(1)}$, thus characterizing the shot-to-shot stability of SC sources [30].

In addition to spectral features, in the following, we also analyze the associated frequency-chirp profile in the temporal domain as a function of fiber length and pump power. Fig. 3a shows the output SC spectra simulated for the same pumping parameters as in Fig. 2a. We clearly see a good agreement about the spectral broadening with increasing input powers, which is confirmed by the comparison of the -20 dB bandwidth depicted in Fig. 3b. A maximum of 140 THz can be reached with a 20 kW input peak power. However, we can note that the simulated SC spectra are flatter than experimental ones, in particular close to the pumping wavelength. In experiments, residual pump energy outside the fundamental mode still propagates in the fiber, thus making here difficult the direct comparison of the -3 dB bandwidths. From numerical simulations, we can expect that the SC pulse at full width half maximum is quasi-linearly chirped over 100 THz. To illustrate and confirm our expectation, Fig. 4 presents the corresponding nonlinear pulse propagation when the input peak power is moderate and fixed to 8.6 kW. We easily observe the SPM-induced spectral broadening in the first steps of propagation (i.e., about 1 cm of propagation) associated with strong (non-monotonic) chirping of the pulse, and a shock front first emerges on the trailing edge due to the self-steepening effect on ultrashort pulses [35] and the dispersion of the nonlinearity. This clearly introduces a strong asymmetry in the pulse dynamics. A typical signature in the spectral domain is the larger spectral broadening on the high-frequency edge as shown in Fig. 4d. Next, one can note that the typical optical wave-breaking takes place. After 3 cm of propagation (see Fig. 4e), the latter helped to flatten the SC spectrum and to linearize the frequency chirp through dispersion. After that, we observe a significant temporal broadening of the pulse to the picosecond range (see Fig. 4f). It appears that only a few-cm-long fiber segments are required at high peak powers to generate positively chirped pulses over 50 THz (−3 dB bandwidth) that can be quasi-linearly compressed to the single-cycle regime (nearly 7 fs pulse duration), while further propagation enhances spectral broadening and flattening. But, it is worth to mention here that the self-steepening effect as well as higher-order dispersions of the tellurite fiber introduce significant asymmetries in the pulse shape and the chirp profile. Both edges of the pulse do not undergo the same dynamics, a pure linear chirp cannot be expected across its entire width. Such a detrimental asymmetry implies that a simple fiber compressor could not provide a full chirp compensation, for approaching the transform-limited pulse. Finally, one can clearly notice that a high degree of coherence is preserved over the full SC spectrum generated in our ANDi tellurite fiber. Similar behaviors were also obtained for the higher input powers under study. This confirms the octave-spanning coherent supercontinuum generation in our step-index tellurite fiber.

3.2. Temporal pulse compression and its optimization

We now investigate the linear compression of our chirped SC pulses by passing them through a dispersive propagation stage. More specifically, we consider the coupling of the pulses into another optical fiber with negative group-velocity dispersion (β_2) in the 2 μm waveband to recombine the frequency components. This simple configuration will have some limitations in terms of compression ratio and pulse quality (i.e., remaining temporal pedestals), however, it provides an all-fibered solution of the complete setup. Advances in fiber splicing technology will allow direct splicing between the different fibers, which would decrease detrimental losses induced by free-space couplings. Step-index fluoride fibers appear as suitable candidates for the linear compression stage in the spectral range under study, since they exhibit excellent transparency, anomalous dispersion, and lower nonlinearity than other infrared-glass optical fibers [36]. Note that few-cycle pulse generation from mid-IR fiber lasers has been recently demonstrated by using a typical grating-fiber compressor [37,38], namely the nonlinear spectral broadening in a short length of step-index chalcogenide fiber and a double-pass diffraction grating pair [15]. For instance, mid-IR pulses as short as 70 fs (7.3 optical cycles) at 2.86 μm were demonstrated. Other techniques based on multi-stage fiber systems rely on nonlinear soliton self-frequency shift or soliton compression [14,39], thus requiring higher initial pulse energies. Here we restrain our study to the simplest configuration based on linear compression with a suitable fiber segment.

In the following, we consider a step-index ZBLAN fiber with a 14 μm core diameter and numerical aperture close to 0.15 (similar features are commercially-available). The corresponding dispersion profile of the fundamental mode is shown in Fig. 1b. It exhibits anomalous dispersion for wavelengths beyond 1.57 μm (i.e., over a wide spectral range of the above SC obtained with the tellurite fiber), its group velocity dispersion at 2.11 μm is $\beta_2 = -35$ ps ^{2} km^{-1}. The large mode area implies a very low nonlinear coefficient below 1 W^{-1} km^{-1}, so that we confirm that nonlinear effects do not occur during the pulse compression stage (i.e., the compression factor does not depend on the power coupled into the fluoride fiber). Typical losses of ZBLAN fibers are known to be about 0.1 dB m^{-1} in the spectral range under study (negligible for fiber segments studied in the following). We performed corresponding numerical simulations on the generalized nonlinear Schrödinger equation that includes the full dispersion curve,

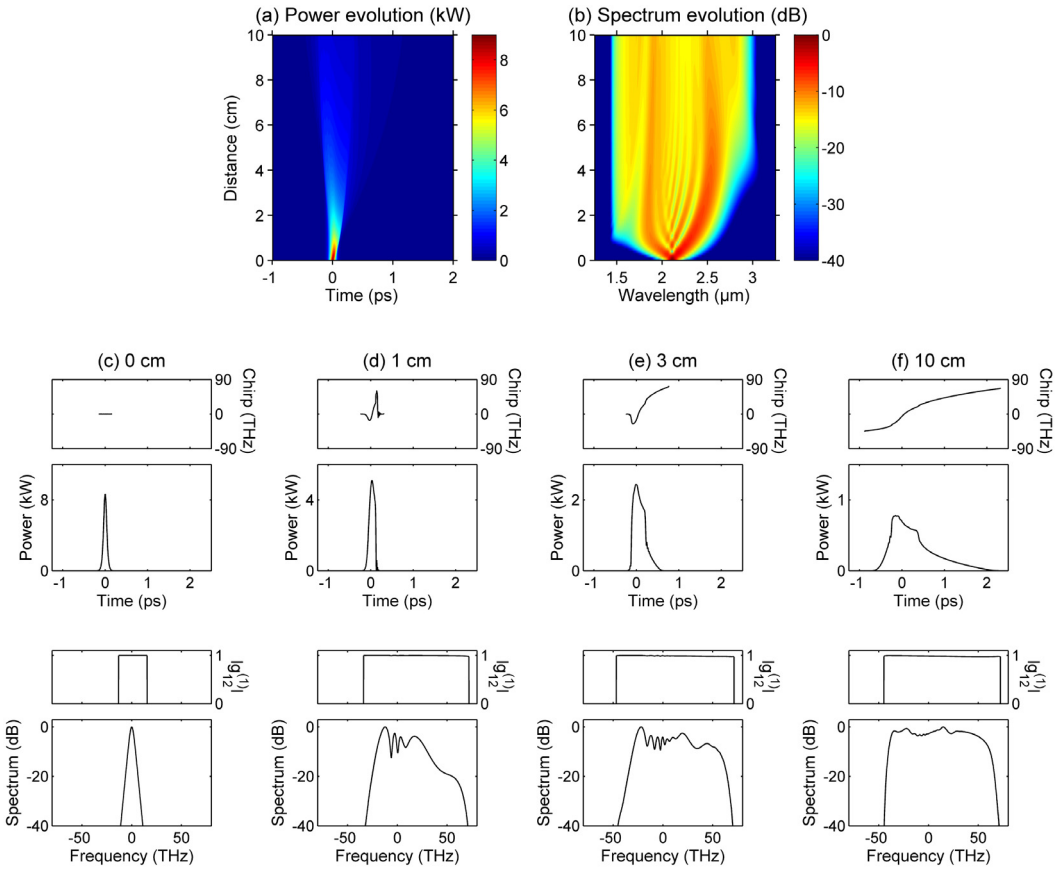

Fig. 4. Simulated nonlinear pulse propagation in our 10-cm-long ANDi tellurite fiber for 8.6 kW input peak power. (a–b) Full evolution of temporal power and power spectrum as a function of propagation distance. (c–f) Power and frequency-chirp profiles in the temporal domain are shown in top panels while the power spectrum and the modulus of the complex degree of first-order coherence in the frequency domain are depicted in bottom panels, for specific propagation distances: (c) 0 cm, (d) 1.5 cm, (e) 3 cm, and (f) 10 cm.

fiber losses, both instantaneous Kerr and delayed Raman nonlinear responses [33]. The action of the fluoride fiber mainly corresponds to a delay line with a frequency-dependent delay [37], thus recombining the frequency components in the opposite direction of that imposed by tellurite dispersion (i.e., leading to the pulse compression). As an example, Fig. 5 shows the evolution of pulse propagation after both tellurite and fluoride fibers when the input peak power at the fiber-system input is fixed to 8.6 kW, as in Fig. 4. The performance of the present all-fiber compressor was solved numerically by optimizing both fiber lengths to obtain the highest peak power at the output [38].

The resulting fiber lengths are respectively: $L_{TZN} = 0.8$ cm and $L_{ZBLAN} = 1.5$ cm. Our all-fiber system is far from being the ideal compressor due to the initial self-steepening effect (see Fig. 5d) and higher-order dispersions in both fibers, it may not necessarily give the best pulse and some uncompressed sidelobes emerge (see Fig. 5e). Nevertheless, we clearly demonstrate that a maximum compressed pulse with 15 fs duration and up to 40 kW peak power can be easily obtained. The central pulse structure is well fitted by a secant hyperbolic shape, and 15% of the total energy here remains in the pedestals.

For our optimization scheme, it appears that the length of nonlinear tellurite fiber has to be shorter than the wave-breaking distance calculated previously ($L_{WB} \sim 1$cm). In contrast to ideal compressors [38], the linearization of the chirp is not required here to reach the maximal compression or to improve the pulse quality, in particular due to the initial asymmetry induced by the self-steepening effect after only 8 mm. When using the simple design rules that govern ideal compressors for initial high N values [37,38], one would obtain a compression factor $F_c \sim N/1.6 \approx 8$, associated to the following fiber lengths of both nonlinear and linear stages: $L_{opt-NL} \sim \sqrt{6 L_{D(TZN)} L_{NL(TZN)}} \approx 2.4$ cm and $L_{opt-Lin} \sim 3T_0^2/(F_c \left|\beta_{2(ZBLAN)}\right|) \approx 2.5$ cm. Such values are not far from those being obtained numerically with the full modeling, and it could give a rough estimate of maximum length required.

Finally, we investigated the optimization of our proposed compressor for the highest peak power that could be injected experimentally in the nonlinear tellurite fiber, namely 20 kW (see Fig. 6). In this configuration, the wave-breaking distance is found to be 0.6 cm and N value is 20. Fig. 6 shows the corresponding pulse propagation, optimized fiber lengths are respectively: $L_{TZN} = 0.4$ cm and $L_{ZBLAN} = 1.1$ cm. The maximum compressed pulse exhibits a 12-fs duration and up to 110 kW peak power (~20% of the total energy remains in the pedestals and the compression factor is 7). We are able to reach again the few-optical-cycle regime of the underlying electric field at 2.11 μm (here, less than 2 optical cycles). One can expect to further compress such pulses down to the single-cycle regime by means of more complex compressors.

4. Conclusion

In summary, we studied experimentally and numerically SC generation in ANDi step-index tellurite fibers. We first demonstrated a 140 THz bandwidth (at −20 dB) SC spectrum in a 10 cm-long tellurite fiber pumped by a turn-key fiber laser emitting 85-fs sech^2 pulses at 2.11 μm at a repetition rate of 19 MHz. Corresponding SC pulses are expected to be quasi-linearly chirped over more than 50 THz. Our numerical study then revealed possibilities of linear compression of such positively chirped pulses in the negative-dispersion region of a large-core step-index fluoride fiber. The main limitation is found to be related to the pulse asymmetry induced by the self-steepening effect during the nonlinear stage. However, we showed that this simple all-fiber compressor scheme, with optimized fiber lengths, allows to reach

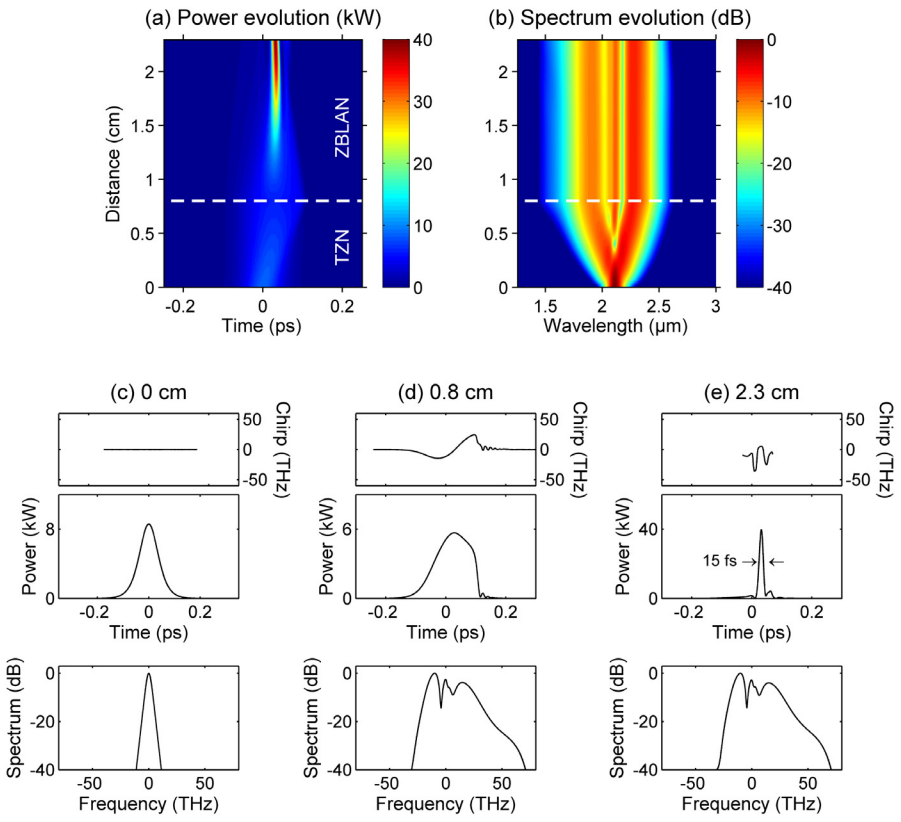

Fig. 5. Simulated nonlinear pulse propagation in our all-fiber compressor for 8.6 kW input peak power. (a–b) Full evolution of temporal power and power spectrum as a function of propagation distance. (c–d) Power and frequency-chirp profiles in the temporal domain are shown in top panels while the power spectrum in the frequency domain is depicted in bottom panels at distinct propagation distances (c) 0 cm, (d) 0.8 cm, and (e) 2.3 cm.

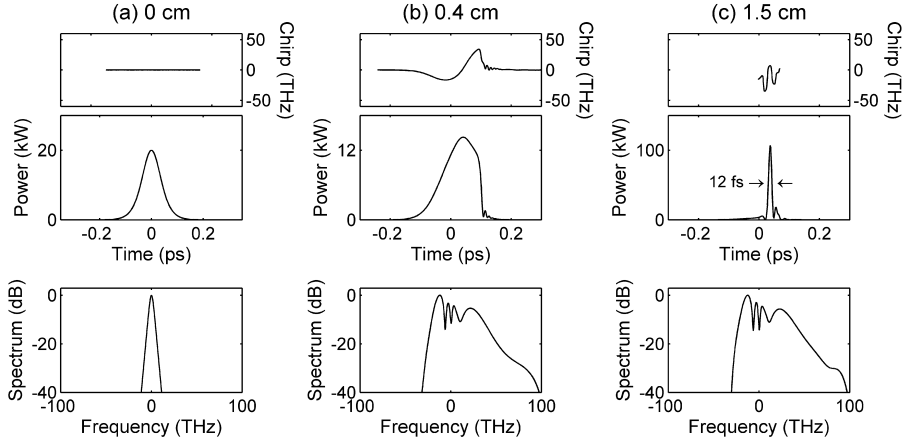

Fig. 6. Simulated nonlinear pulse propagation in our all-fiber compressor for 20 kW input peak power. Power and frequency-chirp profiles in the temporal domain are shown in top panels while the power spectrum in the frequency domain is depicted in bottom panels at distinct propagation distances (a) 0 cm, (b) 0.4 cm, and (c) 1.5 cm.

the few-optical-cycle regime (i.e., down to 12 fs) of the underlying electric field at this wavelength. Our results also confirm that tellurite fibers are suitable candidates for nonlinear frequency conversions in the 2 μm waveband. The development of all-fiber systems is an important step towards the widespread availability of robust mid-IR ultrashort pulse sources.

Declaration of competing interest

The authors declare that they have no known competing financial interests or personal relationships that could have appeared to influence the work reported in this paper.

Funding

This work was supported by the French National Research Agency (ISITE-BFC ANR-15-IDEX-03 Projects SCUVIRA & BRIGHT), the Council of the French Bourgogne Franche-Comté region, and the European program FEDER, through the grant “Jeune Chercheur Entrepreneur”.

References

[1] A.B. Seddon, B. Napier, I. Lindsay, S. Lamrini, P.M. Moselund, N. Stone, O. Bang, M. Farries, Prospective on using fibre mid-infrared supercontinuum laser sources for in vivo spectral discrimination of disease, Analyst 143 (2018) 5874.

[2] F. Borondics, M. Jossent, C. Sandt, L. Lavoute, D. Gaponov, A. Hideur, P. Dumas, S. Février, Supercontinuum-based fourier transform infrared spectromicroscopy, Optica 5 (2018) 378.
[3] I. Zorin, R. Su, B. Heise, B. Lendl, M. Brandstetter, Correlative infrared optical coherence tomography and hyperspectral chemical imaging, J. Opt. Soc. Amer. A 37 (2020) B19.
[4] C.R. Petersen, P.M. Moselund, L. Huot, L. Hooper, O. Bang, Towards a table-top synchrotron based on supercontinuum generation, Infrared Phys. Technol. 91 (2018) 182.
[5] S. Dupont, C. Petersen, J. Thøgersen, C. Agger, O. Bang, S.R. Keiding, IR Microscopy utilizing intense supercontinuum light source, Opt. Express 20 (2012) 4887.
[6] S. Dai, Y. Wang, X. Peng, P. Zhang, X. Wang, Y. Xu, A review of mid-infrared supercontinuum generation in chalcogenide glass fibers, Appl. Sci. 8 (2018) 707.
[7] S. Kedenburg, C. Strutynski, B. Kibler, P. Froidevaux, F. Désévédavy, G. Gadret, J.-C. Jules, T. Steinle, F. Mörz, A. Steinmann, H. Giessen, F. Smektala, High repetition rate mid-infrared supercontinuum generation from 1.3 to 5.3 μm in robust step-index tellurite fibers, J. Opt. Soc. Amer. B 34 (2017) 601.
[8] J. Swiderski, High-power mid-infrared supercontinuum sources: Current status and future perspectives, Prog. Quantum Electron. 38 (2014) 189.
[9] S. Venck, F. St-Hilaire, L. Brilland, A.N. Ghosh, R. Chahal, C. Caillaud, M. Meneghetti, J. Troles, F. Joulain, S. Cozic, S. Poulain, G. Huss, M. Rochette, J.M. Dudley, T. Sylvestre, 2–10μm mid-infrared fber-based supercontinuum laser source: Experiment and simulation, Laser Photonics Rev. 14 (2020) 2000011.
[10] A. Lemière, F. Désévédavy, P. Mathey, P. Froidevaux, G. Gadret, J.-C. Jules, C. Aquilina, B. Kibler, P. Béjot, F. Billard, O. Faucher, F. Smektala, Mid-infrared supercontinuum generation from 2 to 14μm in arsenic- and antimony-free chalcogenide glass fibers, J. Opt. Soc. Amer. B 36 (2019) A183.
[11] J. Hu, L. Mawst, S. Moss, L. Petit, D. Ting, Feature issue introduction: mid-IR optical materials and their device applications, Opt. Mater. Express 8 (2018) 2026.
[12] D. Jung, S. Bank, M.L. Lee, D. Wasserman, Next-generation mid-infrared sources, J. Opt. 19 (2017) 123001.
[13] L.-R. Robichaud, S. Duval, L.-P. Pleau, V. Fortin, S. Toubou Bah, S. Châtigny, R. Vallée, M. Bernier, High-power supercontinuum generation in the mid-infrared pumped by a soliton self-frequency shifted source, Opt. Express 28 (2020) 107.
[14] H. Delahaye, G. Granger, J.-T. Gomes, L. Lavoute, D. Gaponov, N. Ducros, S. Fevrier, Generation of 35 kw peak power 80 fs pulses at 2.9 μm from a fully fusion-spliced fiber laser, Opt. Lett. 44 (2019) 2318.
[15] R.I. Woodward, D.D. Hudson, A. Fuerbach, S.D. Jackson, Generation of 70-fs pulses at 2.86 μm from a mid-infrared fiber laser, Opt. Lett. 42 (2017) 4893.
[16] S.D. Jackson, R.K. Jain, Fiber-based sources of coherent MIR radiation: key advances and future prospects, Opt. Express 28 (2020) 30964.
[17] S. Dupont, Z. Qu, S.-S. Kiwanuka, L.E. Hooper, J.C. Knight, S.R. Keiding, C.F. Kaminski, Ultra-high repetition rate absorption spectroscopy with low noise supercontinuum radiation generated in an all-normal dispersion fibre, Laser Phys. Lett. 11 (2014) 075601.
[18] A.M. Heidt, J. Rothhardt, A. Hartung, H. Bartelt, E.G. Rohwer, J. Limpert, A. Tünnermann, High quality sub-two cycle pulses from compression of supercontinuum generated in all-normal dispersion photonic crystal fiber, Opt. Express 19 (2011) 13873.
[19] S. Xing, S. Kharitonov, J. Hu, C.-S. Brès, Linearly chirped mid-infrared supercontinuum in all-normal-dispersion chalcogenide photonic crystal fibers, Opt. Express 26 (2018) 19627.
[20] S. Kedenburg, T. Steinle, F. Mörz, A. Steinmann, H. Giessen, High-power mid-infrared high repetition-rate supercontinuum source based on a chalcogenide step-index fiber, Opt. Lett. 40 (2015) 2668.
[21] T.S. Saini, T.H. Tuan, X. Luo, N.P.T. Hoa, T. Suzuki, Y. Ohishi, Coherent mid-infrared supercontinuum spectrum using a step-index tellurite fiber with all-normal dispersion, Appl. Phys. Express 11 (2018) 102501.
[22] T.S. Saini, N.P.T. Hoa, T.H. Tuan, X. Luo, T. Suzuki, Y. Ohishi, Tapered tellurite step-index optical fiber for coherent near-to-mid-IR supercontinuum generation: experiment and modeling, Appl. Opt. 58 (2019) 415.
[23] H.P.T. Nguyen, T.H. Tuan, T.S. Saini, X. Luo, T. Suzuki, Y. Ohishi, Highly coherent supercontinuum generation in a tellurite all-solid hybrid microstructured fiber pumped at 2 micron, Appl. Phys. Express 12 (2019) 042010.
[24] T.S. Saini, T.H. Tuan, T. Suzuki, Y. Ohishi, Coherent mid-IR supercontinuum generation using tapered chalcogenide step-index optical fiber: Experiment and modelling, Sci. Rep. 10 (2020) 2236.
[25] C. Strutynski, P. Froidevaux, F. Désévédavy, J.-C. Jules, G. Gadret, A. Bendahmane, K. Tarnowski, B. Kibler, F. Smektala, Tailoring supercontinuum generation beyond 2μm in step-index tellurite fibers, Opt. Lett. 42 (2017) 247.
[26] P. Froidevaux, A. Lemière, B. Kibler, F. Désévédavy, P. Mathey, G. Gadret, J.-C. Jules, K. Nagasaka, T. Suzuki, Y. Ohishi, F. Smektala, Dispersion-engineered step-index tellurite fibers for mid-infrared coherent supercontinuum generation from 1.5 to 4.5μm with sub-nanojoule femtosecond pump pulses, Appl. Sci. 8 (2018) 1875.
[27] C. Strutynski, J. Picot-Clémente, A. Lemière, P. Froidevaux, F. Désévédavy, G. Gadret, J.-C. Jules, B. Kibler, F. Smektala, Fabrication and characterization of step-index tellurite fibres with varying numerical aperture for near- and mid-infrared nonlinear optics, J. Opt. Soc. Amer. B 33 (2016) D12.
[28] F. Désévédavy, C. Strutynski, A. Lemière, P. Mathey, G. Gadret, J.-C. Jules, B. Kibler, F. Smektala, Review of tellurite glasses purification issues for mid-IR optical fiber applications, J. Am. Ceram. Soc. 103 (2020) 4017.
[29] C. Finot, B. Kibler, L. Provost, S. Wabnitz, Beneficial impact of wave-breaking for coherent continuum formation in normally dispersive nonlinear fibers, J. Opt. Soc. Amer. B 25 (2008) 1938.
[30] G. Genty, S. Coen, J.M. Dudley, Fiber supercontinuum sources, J. Opt. Soc. Amer. B 24 (2007) 1771.
[31] A.M. Heidt, Pulse preserving flat-top supercontinuum generation in all-normal dispersion photonic crystal fibers, J. Opt. Soc. Amer. B 27 (2010) 550.
[32] A.M. Heidt, J.S. Feehan, J.H.V. Price, T. Feurer, Limits of coherent supercontinuum generation in normal dispersion fibers, J. Opt. Soc. Amer. B 34 (2017) 764.
[33] Y. Li, L.i Wang, M. Liao, Y.-Y. Liu, X. Li, W. Bi, F. Yu, L. Zhang, Y. Jiang, Z. Wang, L. Zhang, C. Yuan, L. Hu, Step-index fluoride fibers with all-normal dispersion for coherent mid-infrared supercontinuum generation, J. Opt. Soc. Amer. B 36 (2019) 2972.
[34] M.D. O'Donnell, K. Richardson, R. Stolen, C. Rivero, T. Cardinal, M. Couzi, D. Furniss, A.B. Seddon, Raman Gain of selected tellurite glasses for IR fibre lasers calculated from spontaneous scattering spectra, Opt. Mater. 30 (2008) 946.
[35] G.P. Agrawal, Nonlinear Fiber Optics, 6th Ed., Academic Press, 2019.
[36] M. Deroh, J.-C. Beugnot, K. Hammani, C. Finot, J. Fatome, F. Smektala, H. Maillotte, T. Sylvestre, B. Kibler, Comparative analysis of stimulated brillouin scattering at 2 μm in various infrared glass-based optical fibers, J. Opt. Soc. Amer. B 37 (2020) 3792.
[37] W.J. Tomlinson, R.H. Stolen, C.V. Shank, Compression of optical pulses chirped by self-phase modulation in fibers, J. Opt. Soc. Amer. B 1 (1984) 139.
[38] G.P. Agrawal, Applications of Nonlinear Fiber Optics, 2nd Ed., Academic Press, 2008.
[39] J. Huang, M. Pang, X. Jiang, F. Köttig, D. Schade, W. He, M. Butryn, P. St. J. Russell, Sub-two-cycle octave-spanning mid-infrared fiber laser, Optica 7 (2020) 574.